Probing Superexchange Interaction in Molecular Magnets by Spin-Flip Spectroscopy and Microscopy

Xi Chen,[1] Ying-Shuang Fu,[1,2] Shuai-Hua Ji,[1,2] Tong Zhang,[1,2] Peng Cheng,[1] Xu-Cun Ma,[2] Xiao-Long Zou,[1] Wen-Hui Duan,[1] Jin-Feng Jia,[1] and Qi-Kun Xue[1,2,*]

[1]*Department of Physics, Tsinghua University, Beijing 100084, China*
[2]*Institute of Physics, Chinese Academy of Sciences, Beijing 100080, China*

(Received 8 August 2008; published 7 November 2008)

The superexchange mechanism in cobalt phthalocyanine (CoPc) thin films was studied by a low temperature scanning tunneling microscope. The CoPc molecules were found to form one-dimensional antiferromagnetic chains in the film. Collective spin excitations in individual molecular chains were measured with spin-flip associated inelastic electron tunneling spectroscopy. By spatially mapping the spin-flipping channels with submolecular precision, we are able to explicitly identify the specific molecular orbitals that mediate the superexchange interaction between molecules.

DOI: 10.1103/PhysRevLett.101.197208 PACS numbers: 75.75.+a, 68.37.Ef, 75.30.Et, 81.16.Dn

Orbital overlapping, the origin of chemical bonding, magnetism, and so on, generally results in short-ranged interaction between atoms due to the localization of atomic wave functions. To achieve interaction over a large distance, usually the superexchange mechanism [1,2], where a bridging molecule or ion mediates higher-order virtual hopping processes, has to be invoked. The superexchange interaction is responsible for the magnetism in a wide range of materials including transition metal oxides [3] and strongly correlated electronic systems [4]. It also exists in the ultracold atoms in optical lattices [5], as well as in the charge and energy transfer of molecular systems [6]. As a typical superexchange pathway in molecular magnetism [7–9], the nonmagnetic ligands mediate the magnetic coupling between well-separated transition metal ions. Owing to the lack of real-space imaging techniques with high spin sensitivity, the superexchange pathway was usually identified by model calculation.

In the present Letter, we studied the mechanism of superexchange interaction by the spin-flip inelastic electron tunneling spectroscopy (IETS) and microscopy with a scanning tunneling microscope (STM). IETS is one of the most sensitive tools to probe excitations in molecules [10–12]. The latest success of STM-IETS was the measurement of spin excitations, where the tunneling electrons transfer energy to the spin degree of freedom of individual Mn atoms or atomic chains via the spin-flip process [13–15]. Together with external magnetic field, spin-flip spectroscopy provides direct information of spin coupling, and therefore opens new avenues to probe magnetism at the nanometer scale.

The experiments were conducted with a Unisoku ultrahigh vacuum STM at the base temperature of 0.4 K by means of a single-shot ^{3}He cryostat. A magnetic field up to $B = 11$ T can be applied perpendicularly to the sample surface. Pb(111) islands with flat-top surfaces were prepared on the Si(111) $-$ (1×1) $-$ Pb substrate [16,17]. Cobalt phthalocyanine (CoPc) molecules were then thermally sublimed onto the Pb islands at room temperature to form a self-assembled monolayer with square lattice pattern. Subsequent sublimation of CoPc was performed at sample temperature of $\sim$120 K to form the ordered multilayer structures, as shown in Fig. 1(a).

The Co^{2+} ion in a CoPc molecule is coordinated to four pyrrole N atoms [Fig. 1(b)] and has a spin of $S = 1/2$. A CoPc molecule in the first layer is imaged as a uniform four-lobe structure. From the zoom-in STM images [Figs. 1(c) and 1(d)], we determined the stacking geometry of CoPc in the multilayer structures. The Co^{2+} ions of CoPc in the second layers lie directly on the top of those in the first layer, but the in-plane molecular axes is rotated by 45°. From the second to the fifth layers and higher, the planar CoPc molecules are arranged in a columnar fashion. The stacking direction forms an angle of $(60 \pm 3)°$ with respect to the molecular planes [refer to the dashed line in Fig. 1(e)]. Inside a column, a molecule laterally shifts by 2 ± 0.2 Å between neighboring layers so that each Co^{2+} ion lies above or below a pyrrole N atom of the adjacent molecule in the same column.

The scanning tunneling spectroscopy (STS) measurement determines the spin states of the molecules in the first and second layers. Neither the Zeeman splitting nor the Kondo resonance was observed over a molecule directly adsorbed on the Pb surface, suggesting that the magnetic moment of the first molecular layer is completely quenched by the substrate. The spin quenching is further supported by the absence of the spin-induced bound states inside the superconducting gap of Pb [18,19]: the spectrum obtained on the center of a molecule in the first layer is identical to that on the bare Pb surface [Fig. 2(a)].

Similar to the Al_2O_3 and CuN layers that have been used in the past studies [13–15], the first layer of CoPc molecules serves as an insulating buffer to prevent the spins above it from being quenched by the Pb metallic substrate

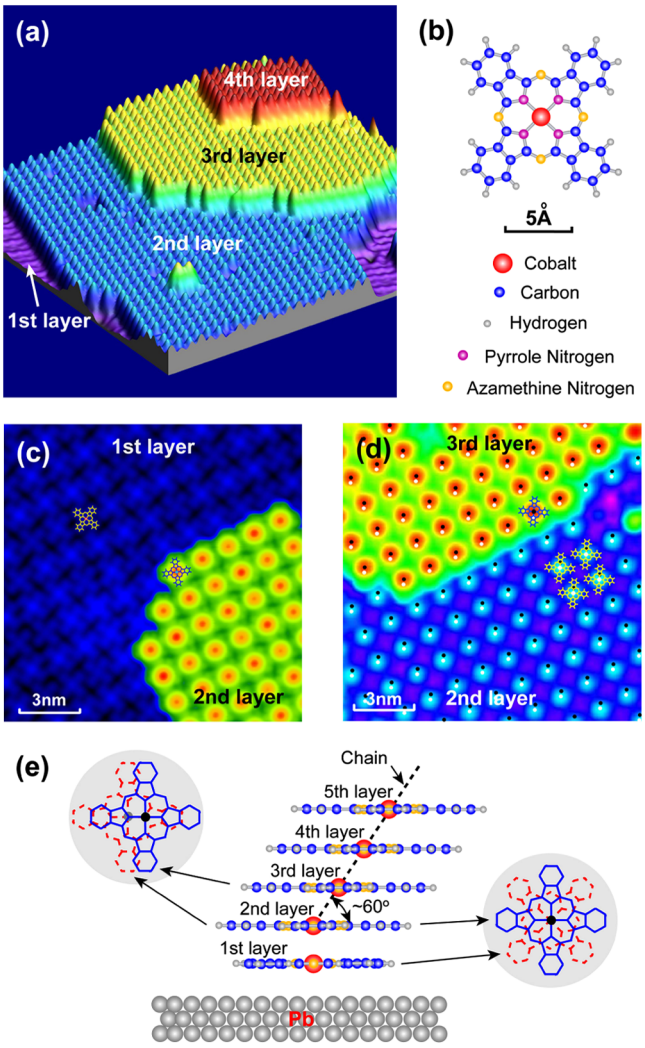

FIG. 1 (color online). CoPc multilayers on Pb. (a) STM image ($V = 0.9$ V, $I = 0.03$ nA) of the self-assembled multilayers of CoPc molecules on Pb(111) film (26 ML thick). (b) Molecular structure of CoPc. (c) STM image ($V = 0.6$ V, $I = 0.1$ A) showing the relative stacking of the 1st and 2nd CoPc layers. (d) STM image showing the relative stacking of the 2nd and 3rd CoPc layers. The white and black dots indicate the centers of the molecules on the 2nd and 3rd layers, respectively. (e) Stacking geometry of CoPc molecules. The molecular layers are spaced 3.5 ± 0.1 Å apart. The inserts show the orientation and displacement between molecules in adjacent layers.

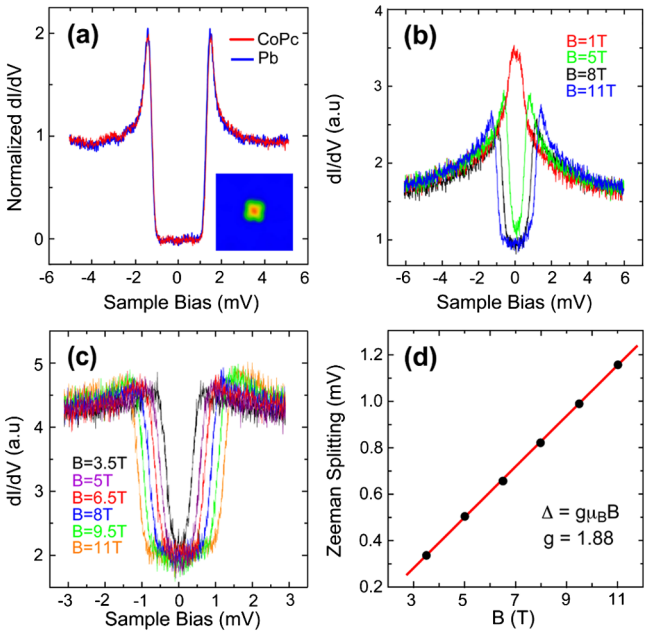

FIG. 2 (color online). STS for molecules in the first and second layers. For all spectra, $T = 0.4$ K and the tunneling junction is set at $V = 6$ mV, $I = 0.2$ nA. The bias modulation was 0.05 mV at 1991 Hz. (a) Superconducting gap observed on bare Pb surface and an isolated CoPc molecule adsorbed on Pb. The insert shows an image of the molecule (8 mV, 0.1 nA). (b) Kondo resonance acquired on a molecule in the second layer. The Kondo peak is split in magnetic field. (c) Zeeman splitting for a molecule away from the top site of the first layer. (d) Magnetic field dependence of the Zeeman energy in (c).

and increase the lifetime of spin excitations. The residual coupling between the substrate and the molecules in the second layer leads to the Kondo effect [17,20] with a Kondo temperature below 10 K. The dI/dV spectra in Fig. 2(b) document the Kondo resonance and its splitting under the magnetic field.

The spin of a molecule on the second layer can be released from the Kondo screening of the substrate by dragging the molecule away from the top sites of the first CoPc layer with the STM tip. A magnetic field is needed to observe the IETS [Fig. 2(c)] of a single CoPc molecule with spin-1/2. Above a threshold bias voltage at E/e (where E is the spin-flip excitation energy and $-e$ is the charge on an electron), tunneling electrons may lose their energy through the spin-flip processes and tunnel inelastically [13–15]. The threshold is represented by a steplike increase in dI/dV at $\pm E/e$. The Zeeman splitting $\Delta = g_\perp \mu_B B$, where μ_B is the Bohr magneton and $g_\perp$ is the Landé g factor in the direction perpendicular to the molecular plane, allows the spin-flip excitation at an energy proportional to the applied magnetic field B. Fitting the data to a line gives $g_\perp = 1.88$ [Fig. 2(d)], which is in good agreement with the ESR measurement [21].

We subsequently detect the spin excitations of the chain-like stacks formed by the CoPc molecules from the second to the fifth layers [Fig. 1(e)] by STS measurements. A magnetic field of 1.5 T was applied to completely quench the superconductive state of Pb. Figure 3(a) shows the dI/dV spectrum at the center (Co^{2+} ion) of a CoPc molecule in the third monolayers. The inelastic tunneling feature [indicated by arrows in Fig. 3(a)] is clearly noted. The single step in Fig. 3(a) splits into three distinct steps [Fig. 3(b)] under magnetic field, suggesting that the observed IETS originates from the antiferromagnetic coupling [22] between two adjacent CoPc molecules in a chain. The split steps correspond to the transitions from the singlet ground

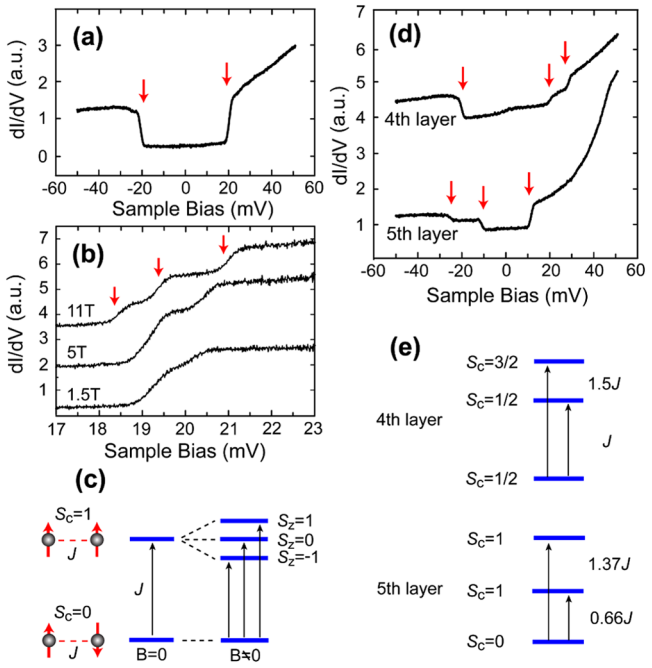

FIG. 3 (color online). Spin-flip spectra of individual CoPc chains. (a) Spectrum acquired with the STM tip positioned on the third molecular layers. The tunneling gap was set at $V = 50$ mV, $I = 0.2$ nA. The bias modulation was 1 mV (rms) at 1991 Hz. The arrows indicate the inelastic tunneling threshold voltages. (b) Spectra on the third layer in different magnetic fields. The STS were acquired at a set point of $V = 10$ mV and $I = 0.15$ nA at $T = 0.4$ K. The arrows indicate the three steps induced by 11 T magnetic field. The lock-in modulation was 0.05 mV at 1991 Hz. (c) Schematic of the spin singlet to triplet transition. The triplet states are labeled by the magnetic quantum number S_z. S_c is the total spin of the chain. (d) Spectra acquired on the fourth and fifth layers. The curves are offset vertically for clarity. (e) Eigenstates of the Heisenberg Hamiltonian ($J > 0$) with $S = 1/2$ and $N = 3, 4$.

state to the triplet excited state whose threefold degeneracy is lifted by the magnetic field as schematically shown in Fig. 3(c). The unequal spacing of the splitting in Fig. 3(c) reflects the effect of magnetocrystalline anisotropy with a barrier height less than 1 meV.

The spin-flip spectra measured on the fourth and fifth layers are displayed in Fig. 3(d). For some transitions, the IETS signals are visible at only one polarity of the bias voltage, possibly due to the asymmetry of the tunneling junction under voltage reversal [23]. The observed spin-flip excitations can be well described by the Heisenberg Hamiltonian

$$H = J \sum_{i=1}^{N-1} \mathbf{S}_i \cdot \mathbf{S}_{i+1} \qquad (1)$$

where $\mathbf{S}_i$ is the spin for the ith site, J is the exchange parameter and N is the number of molecules in the chain. A positive J value corresponds to an antiferromagnetic coupling. Figures 3(c) and 3(e) show the excitation spectra calculated by diagonalizing Eq. (1) with $S = 1/2$. The exchange parameter $J \sim 18$ meV is obtained by comparing the threshold voltages in Figs. 3(a) and 3(d) with the excitation energies of the Heisenberg chain (Table I). J may vary by 10% for different molecules due to the inhomogeneity in the molecular film. All the detectable IETS steps follow the selection rule that $|\Delta S_c| = 0$ or 1, where S_c is the total spin of the chain. The interchain interaction, dominated by noncovalent binding forces, has negligible effect on the magnetic coupling: similar spectra were obtained on a molecule that was dragged out of the ordered molecular layer and placed at any equivalent stacking positions by the STM tip.

The observed antiferromagnetic ordering of the molecular chain is a result of the superexchange interaction, which has been proposed previously to explain the magnetism in MnPc [24,25]. The superexchange interaction arises when an electron of the well-developed π system of phthalocyanine ring hops to the d_{z^2} orbital of a Co^{2+} ion and the remaining unpaired electron on the π orbital enters into a direct exchange with the d_{z^2} orbital of another Co^{2+} [Figs. 4(a) and 4(b)]. As a result, the two adjacent Co^{2+} ions are magnetically linked.

We can resolve the specific molecular orbitals that are involved in the superexchange interaction using the spin-flip imaging together with the first-principles simulation. The bridging orbital in superexchange is magnetically coupled to the central Co^{2+} ion. Therefore, the local electronic density of states of the bridging orbital, which is detected by STS, can be visualized by the dI/dV mapping when the dc bias voltage was fixed at the conductance step [see the spectra in Fig. 4(c)]. The obtained spatial mapping of the inelastic tunneling channels [Fig. 4(d)] is considerably distorted from the D_{4h} symmetry of a CoPc molecule: the charge density is reduced at the benzene ring adjacent to the intervening N atom [indicated by a dashed circle in Fig. 4(d)].

To identify the bridging orbital, we carried out the structural optimizations and total-energy calculations using the DMol^3 package [26,27] within the spin-polarized density functional formalism. The electronic structure of two interacting CoPc molecules indicates that only one orbital with E_g-like symmetry [Fig. 4(e)] can reproduce the spatial distribution of electron density in Fig. 4(d). The overall shape of the dI/dV mapping agrees well with that of the E_g-like orbital, although no details (such as the nodal

TABLE I. Comparison of the spin excitation energies observed by IETS with the calculation based on the Heisenberg model.

N		2	3	4
1st excitation	IETS	18 ± 2	19 ± 2	11 ± 1
energies (meV)	model	18	18	12
2nd excitation	IETS		28 ± 2	25 ± 2
energies (meV)	model		27	25

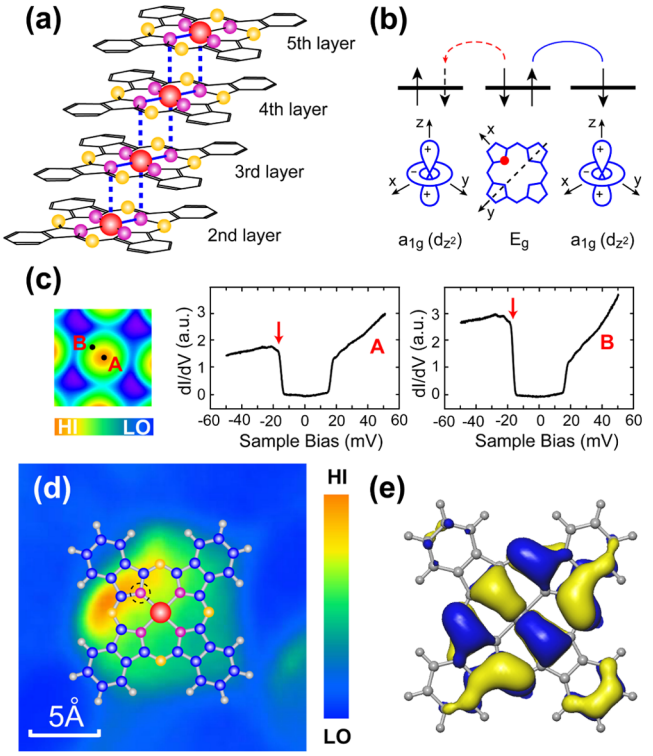

FIG. 4 (color online). Superexchange mechanism. (a) Illustration of the superexchange interaction in a molecular chain. (b) Spin configuration in superexchange. The bridging N atom is marked by a dot. The nodal plane (dashed line) of the E_g orbital passes through two pyrrole N atoms and the central Co^{2+} ion. (c) The spectra at different locations of the molecule. (d) Spin-flip image of a CoPc molecule on the third layer at $T = 0.4$ K. The bias voltage was fixed at -17.2 mV [indicated by arrows in (c)] during mapping. The mapping with positive bias has similar shape, but less contrast. The modulation was 2 mV at 799 Hz. The molecular structure is superimposed on the image. The dashed circle indicates the bridging N atom. (e) Charge density of E_g orbital yielded by the first-principles calculation.

planes) can be resolved due to the spatial resolution limit of STM. The theoretical analysis and experimental measurement suggest that the superexchange pathway involves an E_g orbital of the π system of the phthalocyanine ring, the $3d_{z^2}$ of the same molecule, and the $3d_{z^2}$ of the neighboring molecule.

Molecular magnetic materials show great potential in spin-based electronics and quantum information technology [28–30] as a result of the rich structure of organic chemistry. However, the structure-property relations turn out to be remarkably intricate. The spin-flip spectroscopy and microscopy reported here provide direct information of spin distribution and coupling, and enable our study and understanding of molecular magnetism down to the single molecular level. The information is of great importance for rational design of molecular magnetic materials with desired properties.

This work was supported by National Natural Science Foundation and Ministry of Science and Technology of China. The STM topographic images were processed using WSXM (www.nanotec.es).

*qkxue@mail.tsinghua.edu.cn

[1] H. A. Kramers, Physica (Amsterdam) **1**, 182 (1934).
[2] P. Anderson, Phys. Rev. **79**, 350 (1950).
[3] R. M. White, *Quantum Theory of Magnetism* (Springer-Verlag, Berlin, 2007).
[4] P. A. Lee, N. Nagaosa, and X. G. Wen, Rev. Mod. Phys. **78**, 17 (2006).
[5] S. Trotzky *et al.*, Science **319**, 295 (2008).
[6] V. May and O. Kühn, *Charge and Energy Transfer Dynamics in Molecular Systems* (Wiley-VCH, Berlin, 2001).
[7] O. Kahn, *Molecular Magnetism* (Wiley-VCH, New York, 1993).
[8] J. S. Miller and A. J. Epstein, Angew. Chem.. Int. Ed. Engl., Suppl. **33**, 385 (1994).
[9] J. S. Miller, Inorg. Chem. **39**, 4392 (2000).
[10] R. C. Jaklevic and J. Lambe, Phys. Rev. Lett. **17**, 1139 (1966).
[11] B. C. Stipe, M. A. Rezaei, and W. Ho, Science **280**, 1732 (1998).
[12] X. H. Qiu, G. V. Nazin, and W. Ho, Science **299**, 542 (2003).
[13] A. J. Heinrich, J. A. Gupta, C. P. Lutz, and D. M. Eigler, Science **306**, 466 (2004).
[14] C. F. Hirjibehedin, C. P. Lutz, and A. J. Heinrich, Science **312**, 1021 (2006).
[15] C. F. Hirjibehedin *et al.*, Science **317**, 1199 (2007).
[16] X.-C. Ma *et al.*, Proc. Natl. Acad. Sci. U.S.A. **104**, 9204 (2007).
[17] Y. S. Fu *et al.*, Phys. Rev. Lett. **99**, 256601 (2007).
[18] A. Yazdani, B. A. Jones, C. P. Lutz, M. F. Crommie, and D. M. Eigler, Science **275**, 1767 (1997).
[19] S. H. Ji *et al.*, Phys. Rev. Lett. **100**, 226801 (2008).
[20] A. Zhao *et al.*, Science **309**, 1542 (2005).
[21] J. M. Assour and W. K. Kahn, J. Am. Chem. Soc. **87**, 207 (1965).
[22] A ferromagnetic ground state can not lead to the explicit splitting in Fig. 3(b) at the temperature of 0.4 K.
[23] M. Galperin, M. A. Ratner, and A. Nitzan, J. Phys. Condens. Matter **19**, 103201 (2007).
[24] C. G. Barraclough, R. L. Martin, S. Mitra, and R. C. Sherwood, J. Chem. Phys. **53**, 1638 (1970).
[25] H. Yamada, T. Shimada, and A. Koma, J. Chem. Phys. **108**, 10256 (1998).
[26] B. J. Delley, J. Chem. Phys. **92**, 508 (1990).
[27] B. J. Delley, J. Chem. Phys. **113**, 7756 (2000).
[28] J. Lehmann, A. Gaita-Ariño, E. Coronado, and D. Loss, Nature Nanotech. **2**, 312 (2007).
[29] A. R. Rocha *et al.*, Nature Mater. **4**, 335 (2005).
[30] S. Heutz *et al.*, Adv. Mater. **19**, 3618 (2007).